NASA Contractor Report 177457

An Experimental Investigation of the Chopping of Helicopter Main Rotor Tip Vortices by the Tail Rotor, Part II: High Speed Photographic Study

Charles M. Cary

Contract NAS2-12256
September 1987

NASA

NASA CONTRACTOR REPORT 177457

AN EXPERIMENTAL INVESTIGATION OF THE CHOPPING OF HELICOPTER MAIN ROTOR TIP VORTICES BY THE TAIL ROTOR PART II: HIGH SPEED PHOTOGRAPHIC STUDY

Charles M. Cary
BBN Laboratories Incorporated
Cambridge, Massachusetts 02238

Prepared for:

Ames Research Center
Under Contract NAS2-12256

National Aeronautics and
Space Administration

Ames Research Center
Moffett Field, California 94035

TABLE OF CONTENTS

	Page
LIST OF SYMBOLS	iii
SUMMARY	v
1. INTRODUCTION	1
2. EXPERIMENTAL APPARATUS	2
3. TEST PROGRAM	6
4. EXPERIMENTAL RESULTS AND DISCUSSION	8
5. CONCLUSIONS AND RECOMMENDATIONS	10
REFERENCES	11
FIGURES	12

LIST OF SYMBOLS

b	Number of rotor blades
BPF	Blade passage frequency, Hz
c_R	Rotor chord length, m
c_W	Vortex generator chord length, m
C_T	Rotor thrust coefficient, $T_R/ \rho S (\Omega R)^2$
d	Vortex core diameter, m
$\|\hat{D}\|$	Amplitude of unsteady drag of rotor blade section, Newton
D_o	Free jet nozzle exit diameter, m
D_R	Rotor diameter, m
h/R	Vortex generator tip-rotor tip separation distance normalized with rotor radius, positive for vortex generator tip outside of rotor disk
LE	Leading edge
$\|\hat{L}\|$	Amplitude of unsteady lift of rotor blade section, Newton
M_T	Rotor tip Mach number
p	Pressure, Pascal
$p_{B,F}$	Fluctuating component of blade surface pressure
r/c_W	Radial distance normalized with vortex generator chord length
r/R	Radial distance normalized with rotor radius
r_I/R	Radial blade-vortex interaction station
R	Rotor radius, m
S	Rotor disk area, m^2
SPL	Sound pressure level, dB re 20μPa
t	Time, sec

T_R	Total rotor thrust, Newton
v_i	Induced velocity at rotor disk, m/s
v_θ	Vortex azimuthal velocity, m/s
V_T	Tip speed, m/s
x/c_R	Chordwise distance from rotor blade leading edge normalized with rotor blade chord
u	Velocity component parallel to rotor axis, m/s
U_∞	Free stream velocity, m/s
V_∞	Component of free stream velocity parallel to rotor disk, m/s
α_R	Rotor collective pitch, degree
α_W	Vortex generator geometric angle of attack, degree
β	Blade-vortex interaction angle in a vertical plane, degrees
γ	Blade-vortex interaction angle in a horizontal plane, degrees
Γ	Tip vortex circulation, m^2/s
λ	Rotor inflow ratio, $(U_\infty + V_i)/(\Omega R)$
λ_1	Main rotor chord to tail rotor chord ratio
μ	Advance ratio, $V_\infty/(\Omega R)$
Ω	Rotor radian frequency, rad/s
ρ	Fluid density, kg/m^3
σ	Rotor solidity
θ	Microphone azimuthal position in a horizontal plane, measured from upstream direction, degrees
$\overline{(\quad)}$	Ensemble averaged quantities

SUMMARY

The interaction of a free vortex and a rotor has been recorded photographically using oil smoke and stroboscopic illumination. The incident vortex is normal to the plane of the rotor and crosses the rotor plane at r/R = 0.9. This idealized aerodynamic experiment most nearly corresponds to helicopter flight conditions in which a tip vortex from the main rotor is incident upon the tail rotor while hovering.

The high speed photographs reveal important features not observed using conventional photography where the image is the time average of varying instantaneous images. Most prominent is the strong interaction between the rotor tip vortex system and the incident vortex, resulting in the roll-up of the incident vortex around the (stronger) tip vortices and the resulting rapid destabilization of the deformed incident vortex. The viscous interaction is clearly shown also. Other forms of instabilities or wave-like behavior may be apparent from further analysis of the photographs.

In an earlier project this rotor blade-vortex interaction was characterized in terms of the time-varying pressures on the blade surface and in terms of the radiated sound field produced by the interaction. In this project a clear visualization of the blade-vortex interaction has been accomplished.

1. INTRODUCTION

Blade-vortex interaction (BVI) in helicopters results in undesirable levels of impulsive noise, as well as aerodynamic loadings which contribute to stress, fatigue, and vibration. While the parallel interaction problem, which occurs between main rotor blades and main rotor tip vortices, has been given much attention, only a few researchers (Refs. 1-6) have studied the normal incidence problem, which can occur when the main rotor tip vortex is convected into the tail rotor.

The present study continues an earlier study (Ref. 6) in which the BVI at normal incidence was characterized by the directional sound field and blade surface pressures, while varying parameters such as tip Mach number and rotor incidence station. In this work we have made high speed still photographs of the incident vortex during BVI to further the understanding of this complex phenomenon.

2. EXPERIMENTAL APPARATUS

2.1 Wind Tunnel

The experiments were conducted in the high-speed acoustic wind tunnel at Bolt Beranek and Newman Inc. (BBN) in Cambridge. The facility is described in some detail in Refs. 7 and 8. The tunnel was configured as an open-jet for the experiments. The free jet emerges from a 1.378m diameter nozzle into a 7m x 13m x 6m test chamber, as shown in Figure 1. The tunnel can be operated in either open- or closed-circuit mode. For the present tests, it was operated in open-circuit mode to prevent the buildup of temperature and smoke.

The tunnel, which is powered by a 600 hp diesel engine, can reach a maximum velocity of about 45 m/s with the 1.49 m^2 round nozzle used in the present tests. The overall turbulence level is 0.23%. In the present experiments, the tunnel was operated at an extremely low power level as required by the test condition velocity. The walls of the chamber are covered with foam providing a cut-off frequency of 160 Hz.

The facility is equipped with a sting-mounted rotor spinner capable of operating at speeds up to 9000 rpm. The unit is driven by a hydraulic motor (maximum power output of 15 hp). The spinner was aligned with the free jet axis, at a height of 2.4m above the chamber floor (Figure 2).

2.2 Model Rotor and Vortex Generator

Rotor Similarity Parameters

Reference 6 describes the establishment of a set of test conditions which satisfied the similiarity parameter ranges given below.

1. Rotor tip speed, V_T = 183 - 213 m/s
2. Advance ratio, $\mu = V_\infty/(\Omega R) = 0 - 0.4$
3. Blade loading, C_T/σ = 0.1 max
4. Disk loading, T_R/S = 239 - 479 Pa
5. Inflow ratio, $\lambda = (U_\infty + v_i)/(\Omega R) = 0.05 - 0.1$ (hover)

Here V_∞ is the component of free stream velocity parallel to the rotor disk, $C_T = T_R/[\rho\pi R^2(\Omega R)^2]$ is the rotor thrust coefficient and $\sigma = bc/\pi R$ is the rotor solidity. To encourage aerodynamic similarity by minimization of Reynolds number effects, boundary layer trip strips were installed on the suction and pressure

sides of the blades. The tripping device consisted of strips of pinked tape 0.2 mm in thickness installed at the quarter chord position. This device has been described in Refs. 9 and 10.

To match the rotor similarity parameters, rotor thrust was calculated using the extended blade-element theory of Ref. 11 with Prandtl-Betz tip loss correction and Prandtl-Glauert compressibility correction. Ref. 6 established good agreement between these aerodynamic results and those of the lifting-surface theory of Ref. 12 with Prandtl-Glauert compressibility correction.

For the present test configuration $V = 0$. Hence, the rotor advance ratio $\mu = 0$ for all conditions tested.

Rotor/Vortex Generator Relative Size and Spacing

Relative size of the model rotor and vortex generator was determined from a survey of light helicopters with two-bladed tail rotors. Parameters of interest were tail rotor solidity σ, blade aspect ratio AR, and the ratio of main rotor chord to tail rotor chord λ_1. The selected values were approximately the average values from the survey: $\sigma = 0.127$, AR = 5.00, and $\lambda_1 = 2.75$.

According to the wake rollup theory of Ref. 13, the wake of the vortex generator is essentially rolled up at a distance of 2.5 c_w downstream of the trailing edge. Smoke emitted from the vortex generator tip visually confirmed the rollup. Earlier hot wire volicity measurements (Ref. 6) showed at compact vortex at three chord lengths. Therefore, the model rotor was placed three chord lengths downstream of the vortex generator trailing edge.

Model Rotor

Since the goal of the present work was to gain a better understanding of blade-vortex interaction at normal incidence, a simple generic model rotor was designed and constructed, with the following characteristics:

- Number of blades: 2
- Diameter: 0.610m
- Blade section: NACA 0012
- Blade planform: rectangular
- Twist: 0
- Collective pitch: 9° (fixed)
- Chord length: 6.10 cm (constant)
- Blade tip: flat (square cutoff)
- Blade aspect ratio: 5
- Rotor solidity: 0.127

- Direction of rotation: CW looking upstream
- Hub diameter: 6.4 cm

Selection of a design with constant collective pitch followed the determination in Ref. 5 of low sensitivity of blade-vortex interaction noise to blade collective pitch.

Vortex Generator

The vortex generator consisted of a semi-span wing with the following characteristics:

- Airfoil section: NACA 0012
- Planform: rectangular
- Twist: 0
- Span: 0.8 m
- Chord: 16.8 cm (2.75 times rotor blade chord)
- Tip geometry: rounded (NACA 0012 half body of revolution)

The vortex generator was mounted on a support system which allowed it to be moved vertically to adjust the blade-vortex interaction station r_I/R and rotated to adjust its angle of attack.

To prevent laminar separation and aerodynamic dissimilarity, a boundary layer trip strip similar to that on the rotor was placed on the vortex generator. A row of tufts on the suction side near the trailing edge provided a visual check for fully attached flow. An internal tube carried the smoke to the tip of the vortex generator where it was injected into the evolving vortex core.

2.3 Instrumentation

Velocity Measurements

During the experiments the rotor speed and the tunnel air speed were monitored continuously. The rotor speed was measured using a Hall-effect sensor and a frequency counter. The tunnel speed was measured at the exit of the nozzle using a standard pitot-static tube and a Celesco transducer with 0.1 psi diaphragm.

Acoustic Measurements

The acoustic signature of the blade-vortex interaction was measured at two locations, 50° and 130° (see Fig. 2) using 1.27 cm (1/2 in.) B&K microphones.

Pressure Measurements

Two pressure transducers on the rotor,one at r/R = 0.9 on the low pressure side and one at r/R = 0.975 on the high pressure side, were monitored initially to confirm the established test condition.

Flow Visualization and Photography

Visualization of the incident vortex during interaction with the rotor was essential to this effort.

A Cloud Maker smoke generator, built for theatrical applications, was modified for experimental use. The smoke was carried through silicone rubber tubing to an opening at the vortex generator tip on the low pressure side adjacent to the tip fairing, at about the three-quarter chord position. At the low point in the tubing, a thistle jar was installed to collect condensed vapor which otherwise led to erratic smoke ejection rates. At the vortex generator tip, the emerging smoke was entrained by the evolving tip vortex.

The visualized blade-vortex interaction was photographed using a Nikon single lens reflex camera with 80 mm to 210 mm variable focal length lens. Illumination and motion freezing was provided by a General Radio stroboscope with a flash duration of less than 1/2000 second yielding excellent clarity. The stroboscope was triggered by a photocell pickup with adjustable delay. The position of the blade in the photographs was achieved by manual adjustment of the delay and visual comparison of the strobed rotor to a target.

Preliminary photographs were made with a Polaroid-backed camera to establish exposures. During final shooting a trial roll of film was used to determine development corrections for the Kodak Tri-X film.

3. TEST PROGRAM

3.1 Test Condition

The test condition was the same as condition 2 in Ref. 6:

$M_T = 0.59$

$U_\infty = 8.2$ m/s

$\alpha_w = 13.3°$

$r_I/R = 0.90$

3.2 Verification Tests

With the geometric and kinematic conditions established, it remained to verify that the radiated sound field of the BVI and the rotor blade surface pressures corresponded to those measured in Ref. 6 at the same test condition. Accordingly, sound measurements were made at $\theta = 50°$ and $\theta = 130°$, at a distance of 1.5m, and blade surface pressure measurements were made at $r/R = 0.90$ and at $r/R = 0.975$.

3.3 Photography

Two photographic investigations were carried out. The second, more detailed than the first, was substituted for a velocity measurement task which could not have been done with single or double (45° crossed) hot wires because (1) the flow possesses three significant orthogonal components, and (2) the velocity vector departs more than 45° from the axial direction in a large neighborhood of the rotor tip vortex system.

The first set of high speed photograph measurements was superceded by the second, but was important to understanding the essential problems with the proposed velocity measurement. In addition to black and white high speed still photographs, a videotape recording of the blade-vortex interaction was made to assist the interpretation of the still photographs. The videotape shows the interaction in synthetic slow motion, which was obtained by running the strobe continuously and slowly varying delay. Since the strobe flashed about four times per VCR frame, the VCR images lack the clarity achieved in the still photographs.

The second set of photographs was taken from three viewing positions at ten rotor positions. A 25.4 mm (1.0 in.) grid was also photographed to be used as an overlay for measurement purposes. For each view, the camera was not changed in any way

between frames, so that the relative positions of the interaction phenomena can be accurately measured with the grid. The three viewing positions were (1) looking horizontally in the plane of the rotor (approximately perpendicular to the rotor leading edge at the instant of incident vortex interception), (2) same as (1) but 45° downstream from the rotor disk, and (3) looking vertically upward in the plane of the rotor disk (approximately in line with the rotor leading edge at the instant of interception). In all cases, the lens focal length was 210 mm. The ten rotor positions with respect to incident vortex interception were -5°, 0°, 5°, 10°, 15°, 20°, 30°, 60°, 90°, and 120°. Interception here is defined as that position when the leading edge is at the center of the incident vortex, as determined visually. The strobed rotor was moved sequentially to the ten positions using the delay control. At each position at least one photograph was taken.

To ensure high quality images on the film, extra film was shot for development trials. The resulting negatives have good contrast, density, and clarity.

4. EXPERIMENTAL RESULTS AND DISCUSSION

4.1 Validation Measurements

Acoustic Waveforms

At the test condition, time histories of the acoustic pressure were recorded at 50° and 130°, with the vortex generator at 13.3° and at 0°. The difference between the acoustic pressure with the vortex generator at 13.3° and the acoustic pressure with the vortex generator at 0° is termed the acoustic signature of the blade vortex interaction. The BVI acoustic spectra and acoustic signatures recorded here are compared with those recorded in the previous experiment at $\theta = 50°$ and $\theta = 130°$ in Figs. 3a through 3f. Qualitative agreement is very good. In the present experiment acoustic conditions in the wind tunnel were not identical to those in the earlier study, because acoustic treatments for the floor and hardware were not used, causing differences in the background noise level. The essential interaction signature was reproduced. The waveforms show somewhat lower amplitudes even though all kinematic conditions were satisfied.

Blade Pressure Waveforms

At the test condition, time histories of the surface pressure on the rotor at $r/R = 0.975$ on the pressure side and at $r/R = 0.9$ on the suction side were recorded and are compared with the previously reported surface pressures in Figs. 4a and 4b. Background noise is greater in the present results because no averaging was done. The BVI peaks have a clipped appearance which reduces the maximum pressure amplitude, but the event has a very similar width. The clipping was not a result of the electronics, but could have been caused by a larger core diameter of the incident vortex.

4.2 High Speed Photographs

Side View

The set of photographs taken from the side is shown in Figs. 5a through 5k. The camera was in the rotor plane and approximately perpendicular to the leading edge at the instant of chopping. The camera position did not change and subsequent photoprocessing was indexed to the film sprocket holes, so that the position of the BVI has no motion component due to recording, processing, or reporting of the data. The 25.4 mm (1.00 in.) grid in Fig. 5a may be overlayed to show the motion of the incident vortex as it is chopped by the blade as it comes under the influence of the rotor tip vortex system. In the sequence

the position of the leading edge of the vortex with respect to the incident vortex is -5°, 0°, 5°, 10°, 15°, 20°, 30°, 60°, 90° and 120°.

45° Oblique View

When viewed from a point which is displaced downstream 45° from the side viewpoint, the blade-vortex interaction appears as shown in Figs. 6a through 6l. The grid in Fig. 6a is perpendicular to the camera axis, while the grid in Fig. 6b is parallel to the tunnel axis. The grid spacing is 25.4 mm (1.00 in.). In the sequence the blade is positioned at -5°, 0°, 5°, 10°, 15°, 20°, 30°, 60°, 90°, and 120°.

Bottom View

In this view the blade is viewed end-on at the instant of interception. Visualization of the blade vortex interaction for this view is shown in Figs. 5a through 5k. The blade is at -5°, 0°, 5°, 10°, 15°, 20°, 30°, 60°, 90°, and 120° sequentially with respect to the instant of vortex chopping.

Discussion

Clearly the rotor tip vortex system causes large scale distortion of the incident vortex. The resulting wind-up is essentially perpendicular to the tip vortex and therefore plainly visible in the side view, while not at all visible in the bottom view. There is a separated wake at r/R = 0.9 which shows up in the bottom view but is hidden in the side view. Chordwise circulation at r/R = 0.9 produces the relative displacement of the incident vortex seen in the bottom view.

The incident vortex has turbulent structures, which can be seen in all of the photographs. As the incident vortex passes through the rotor plane, it is initially stretched by the rotor tip vortex system, causing a smoothing and reduction in diameter. The stretched and curved vortex then appears to develop thin spots or holes. Where the incident and vortex is interrupted by the rotor viscous wake, the vortex disintegrates rapidly.

The BVI noise phenomenon has been considered to be caused in large part by the unsteady but linear loading due to the vector sum of the incident vortex velocity and the steady blade surface velocities with non-separated flow. In light of these photographs, BVI noise may be partially the result of transient stall in the vicinity of the incident vortex. In the bottom view, a substantial rotor viscous wake is evident.

5.0 CONCLUSIONS AND RECOMMENDATIONS

We have modelled the interaction of a helicopter main rotor tip vortex with a tail rotor. The incident vortex was normal to the rotor plane and the experimental conditions are similar to the hovering mode. The incident vortex has been visualized with oil smoke and successfully photographed using high speed stroboscopic illumination.

The complex interaction between the incident vortex and the stronger rotor tip vortex system is not presently amendable to theoretical analysis. As the rotor blade cuts the incident vortex, it leaves a viscous wake and causes a dislocation proportional to rotor circulation. Both prevent the reconnection of the incident vortex after the cut has taken place. Consequently, the incident vortex diffuses rapidly on both sides of the cut. The rotor tip vortex introduces curvature to the incident vortex, which further destabilizes it. One aerodynamic pitch downstream, the incident vortex has lost most of its coherence.

The substantial amount of separation evident from the bottom view may influence the noise generation characteristics of blade-vortex interaction. While the constant pitch angle rotor design is typical of tail rotors, greater understanding of the aerodynamics and aeroacoustics of this phenomenon may be possible using a rotor with constant induced pitch.

Better flow visualization would result from the use of a high speed motion camera. Sequential frames would be correlated in time, unlike those in this report which are separated by large random amounts of time. The destabilization of the incident vortex could be viewed in slow motion.

Velocity measurements would be useful. The recommended measurement program would require the development of miniature three-wire probes and a microprocessor-driven system for data acquisition, storage, and reduction.

REFERENCES

1. Schmitz, F.H. and Yu, Y.H. (1983), "Helicopter Impulsive Noise: Theoretical and Experimental Status," NASA TM-84390.

2. White, R.P., Balcerak, J.C. and Pegg, R.J. (1976), "A Parametric Model Study of the Noise Generated by the Aerodynamic Interaction of the Tail Rotor with the Wake of the Main Rotor," AHS Mid-East Region Symposium of Rotor Technology, Essington, PA.

3. Leverton, J.W., Pollard, J.S., and Willis, C.R. (1977), "Main Rotor/Tail Rotor Interactions," Vertica, Vol. 1, No. 3, pp. 213-221.

4. Pegg, R.J. and Shidler, P.A. (1978), "Exploratory Wind Tunnel Investigation of the Effect of the Main Rotor Wake on Tail Rotor Noise," NASA CP- 2052, Part 1, pp. 205-219.

5. Schlinker, R.H. and Amiet, R.K. (1983), "Tail Rotor Blade-Vortex Interaction Noise," AIAA Paper 83-0720.

6. Ahmadi, A.R. (1984), "An Experimental Investigation of the Chopping of Helicopter Main Rotor Tip Vortices by the Tail Rotor," NASA CR177338.

7. Kadman, Y. and Hayden, R.E. (1976), "Factors in the Design and Performance of Free-Jet Acoustic Wind Tunnels," Progress in Astronautics and Aeronautics, Vol. 46, pp. 247-258.

8. Hayden, R.E. and Theobald, M.A. (1982), "Aeroacoustic Facility Installation Effects on the Generation and Propagation of Propeller-Generated Noise," BBN Report No. 5126.

9. Hama, F.R. (1957), "An Efficient Tripping Device," J. Aeronautical Sci., 24, pp. 236-237, March.

10. Paterson, R.W. and Amiet, R.K. (1979), "Noise of a Model Helicopter Rotor Due to Ingestion of Turbulence," NASA CR-3213.

11. Gessow, A. and Myers, G.C., Jr., (1952), Aerodynamics of the Helicopter, Ungar Publishing Co., New York.

12. Greeley, D.S. and Kerwin, J.E. (1982), "Numerical Methods for Propeller Design and Analysis in Steady Flow," SNAME Transactions, Vol. 90, pp. 415-453.

13. Spreiter, J.R. and Sacks, A.H. (1951), "The Rolling Up of the Trailing Vortex Sheet and Its Effect on the Downwash Behind Wings," J. Aeronautical Science, January.

ORIGINAL PAGE IS
OF POOR QUALITY

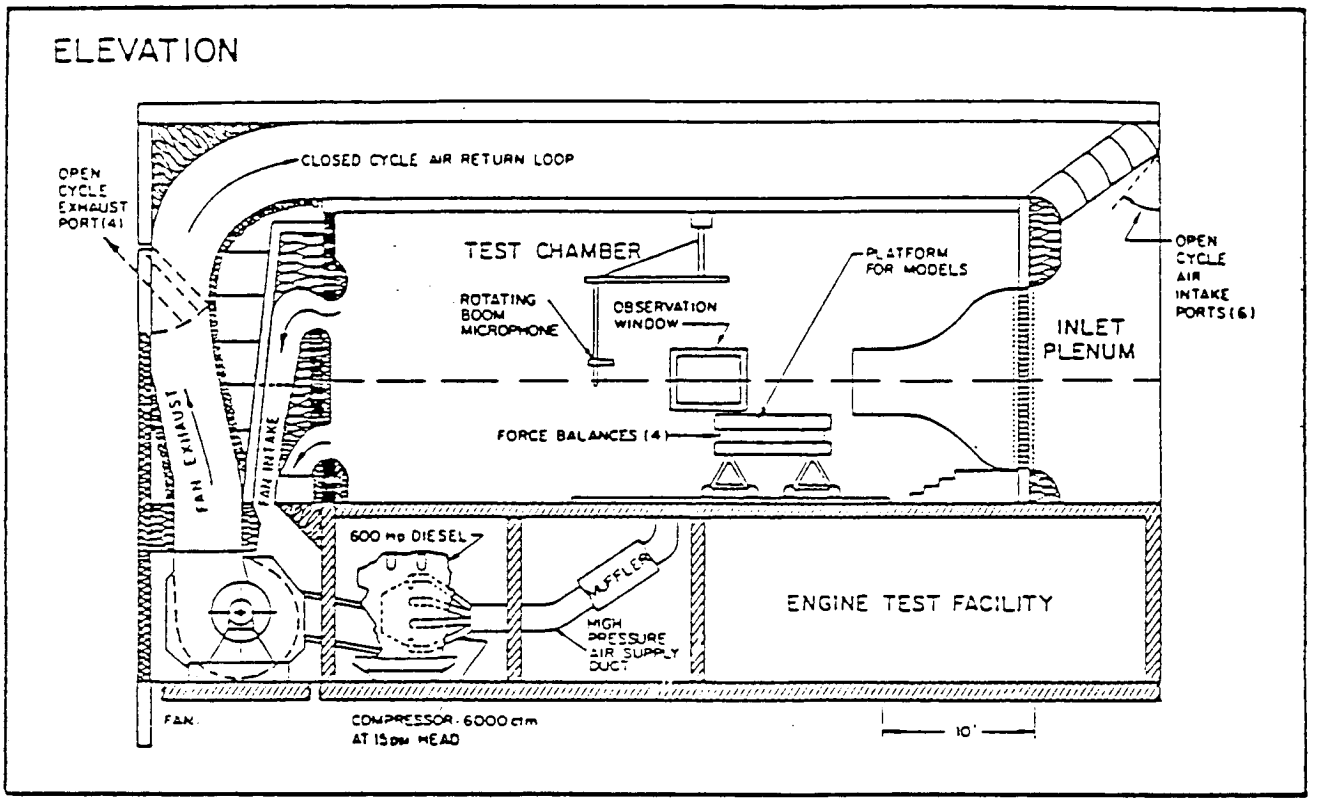

FIG. 1. BBN HIGH SPEED ACOUSTIC WIND TUNNEL (ELEVATION).

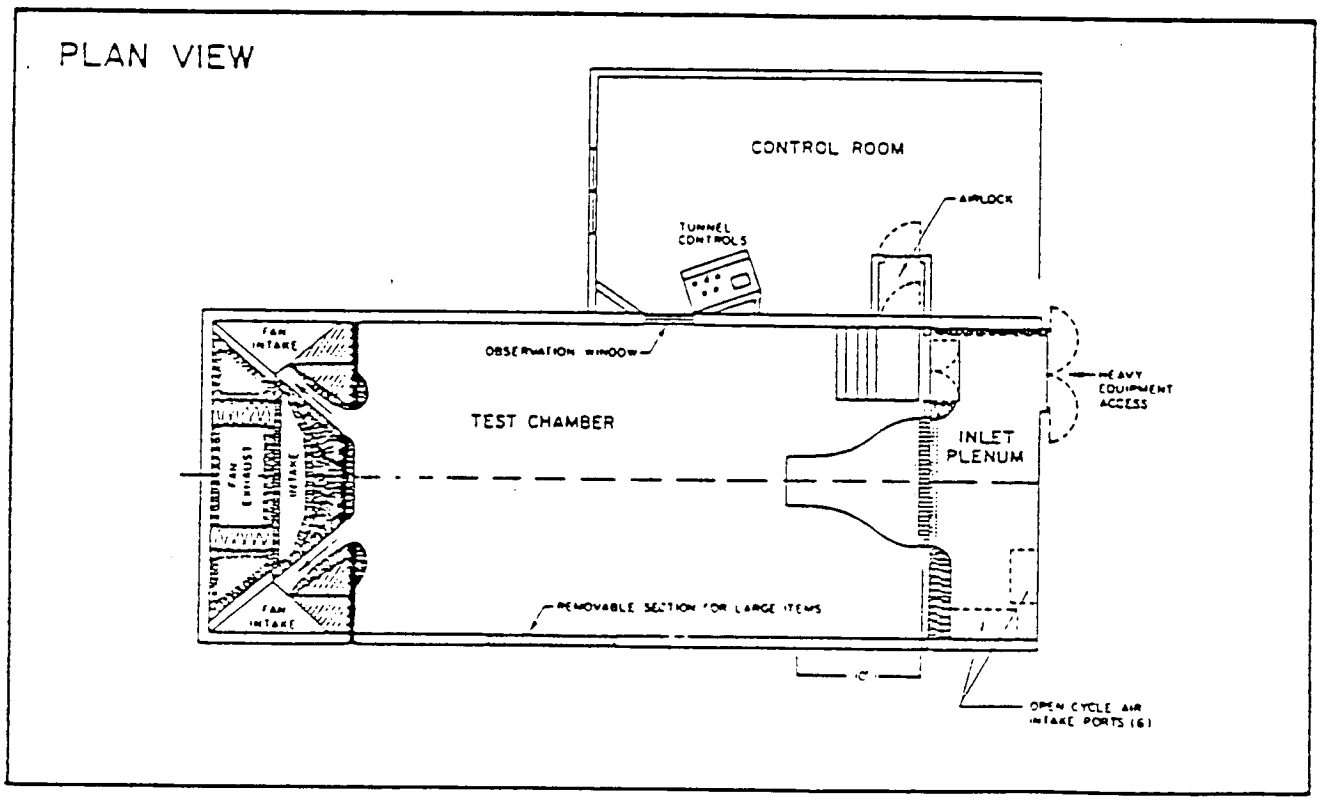

FIG. 1a. BBN HIGH SPEED ACOUSTIC WIND TUNNEL (PLAN VIEW).

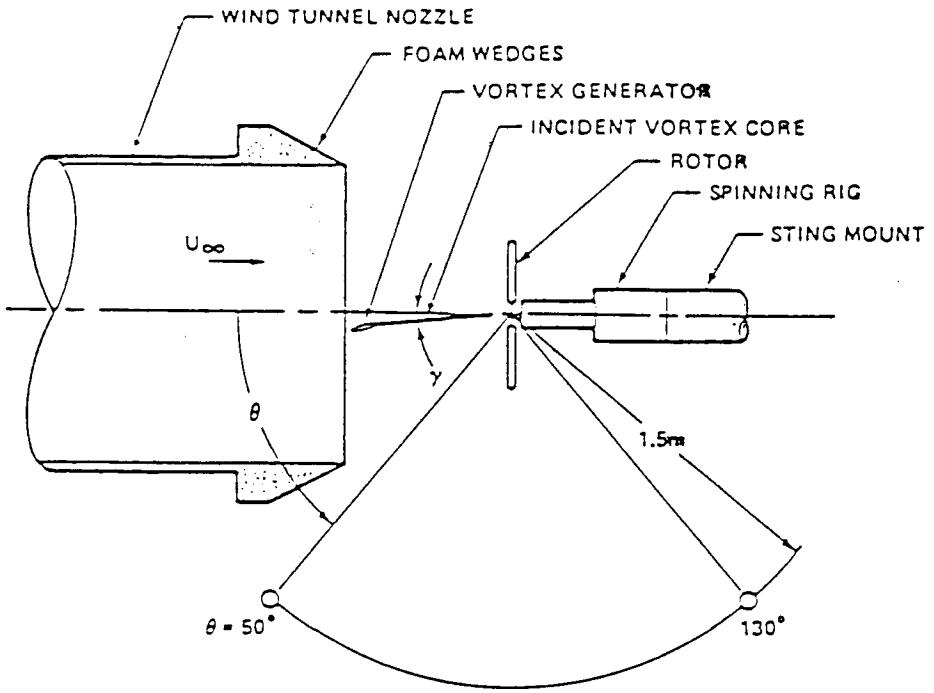

a) Planview

FIG. 2a. EXPERIMENTAL ARRANGEMENT OF BVI INVESTIGATION (Planview)

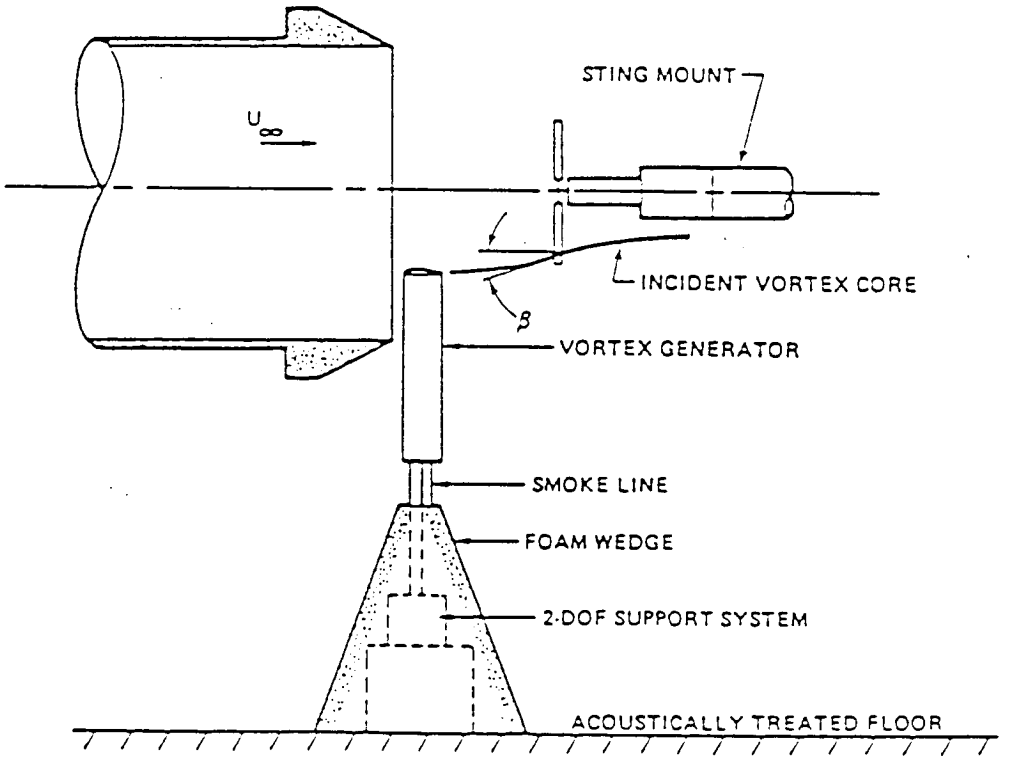

b) Sideview

FIG. 2b. EXPERIMENTAL ARRANGEMENT FOR BVI INVESTIGATION (Sideview).

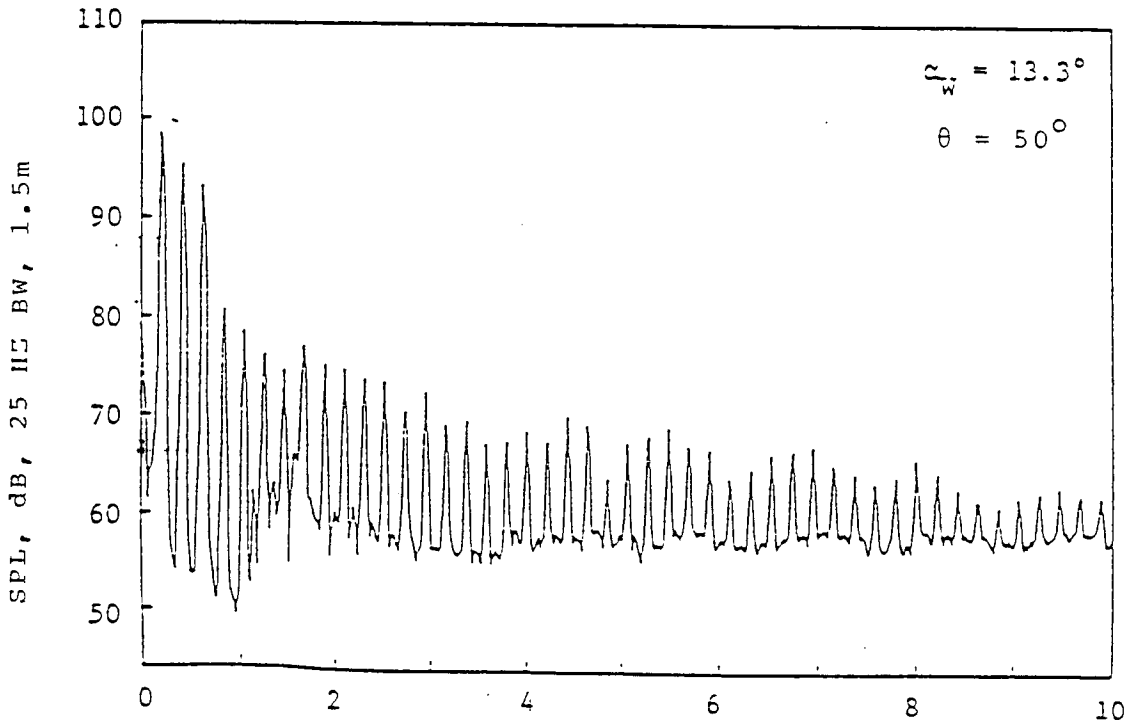

(1) EARLIER STUDY (REF. 6).

FIG. 3a: COMPARISON OF ACOUSTIC SPECTRA AT $\theta = 50^{\circ}$, $\alpha_w = 13.3^{\circ}$

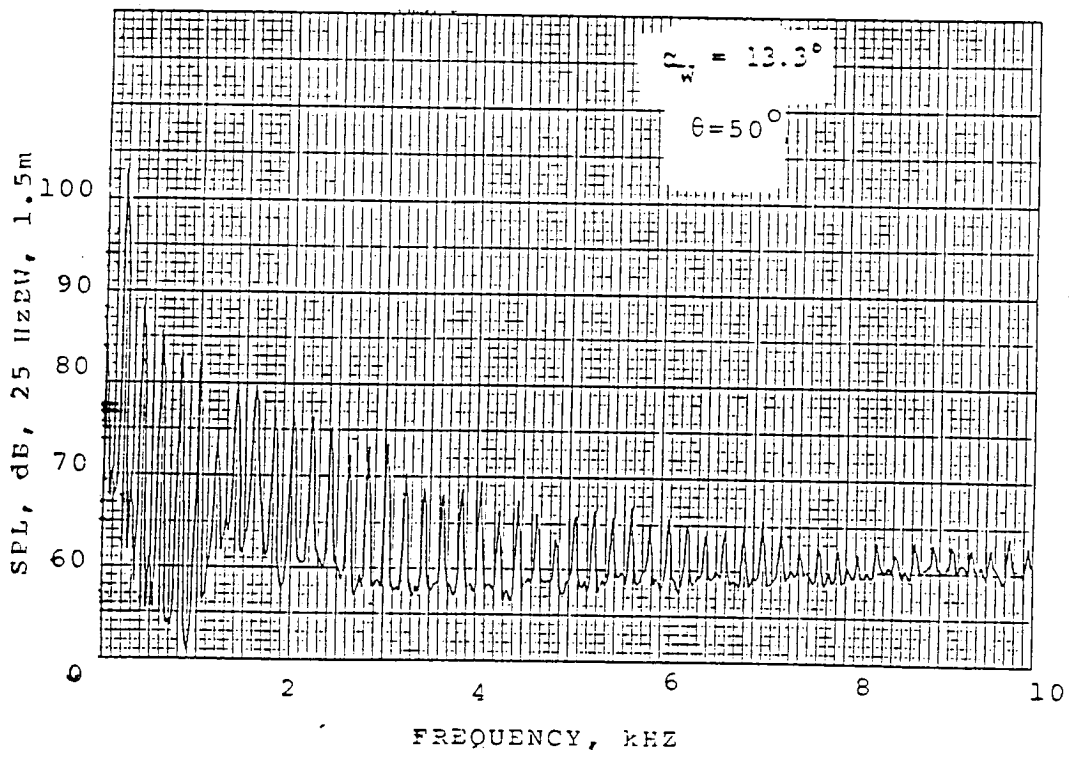

(2) PRESENT STUDY.

FIG. 3a: COMPARISON OF ACOUSTIC SPECTRA AT $\theta = 50^{\circ}$, $\alpha_w = 13.3^{\circ}$ (continued)

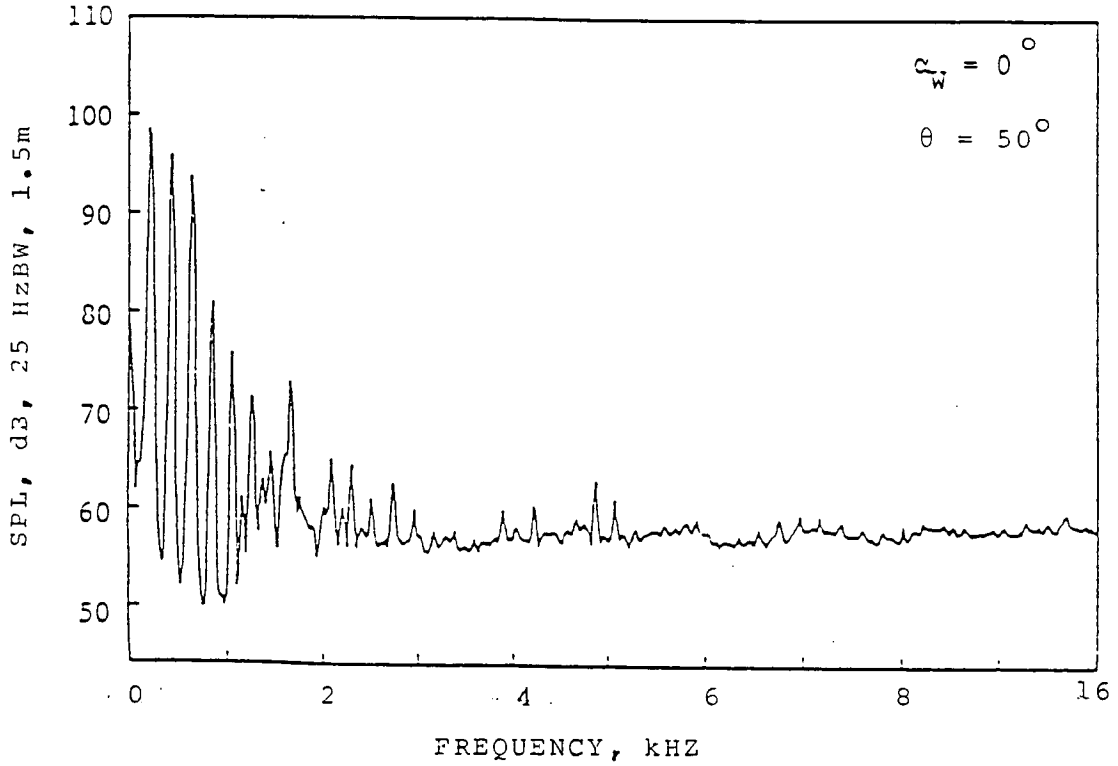

(1) EARLIER STUDY (REF. 6).

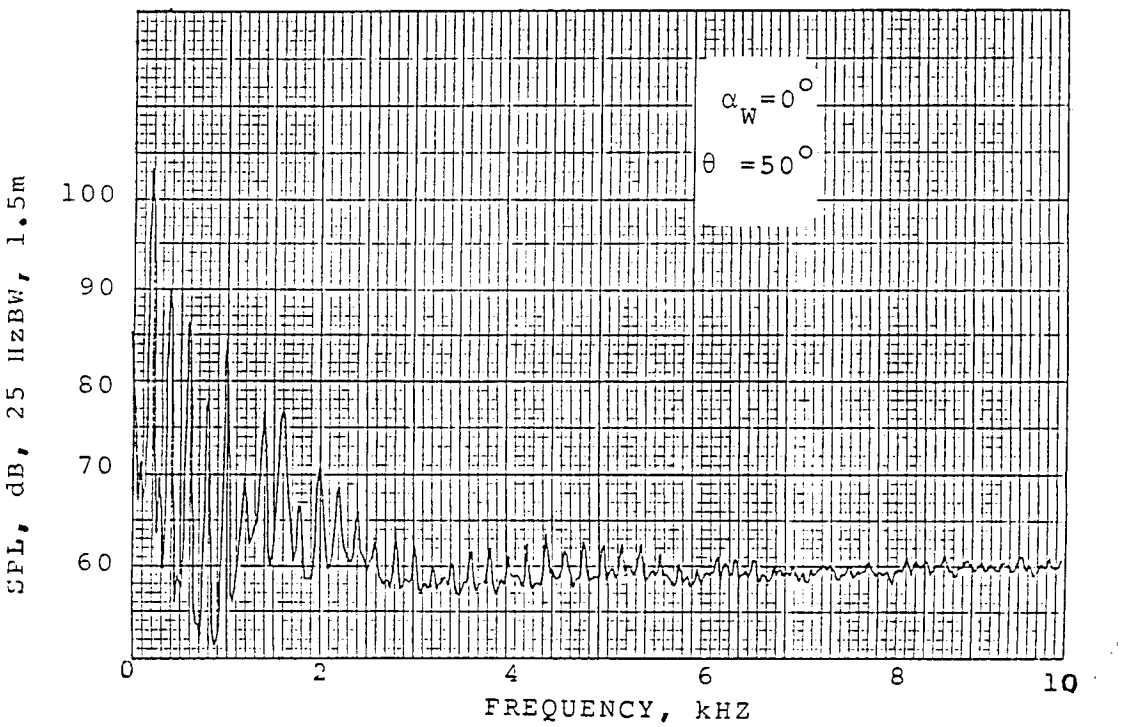

(2) PRESENT STUDY.

FIG. 3b: COMPARISON OF ACOUSTIC SPECTRA AT $\theta = 50^\circ$, $\alpha_w = 0^\circ$

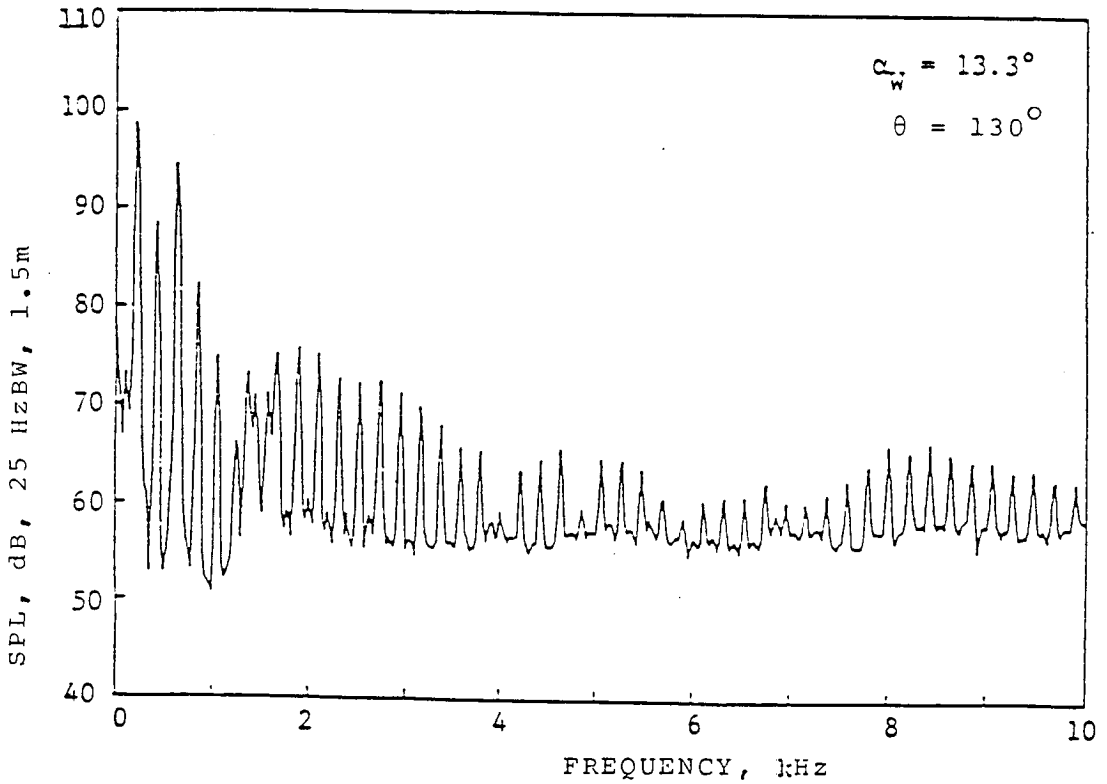

(1) EARLIER STUDY (REF. 6).

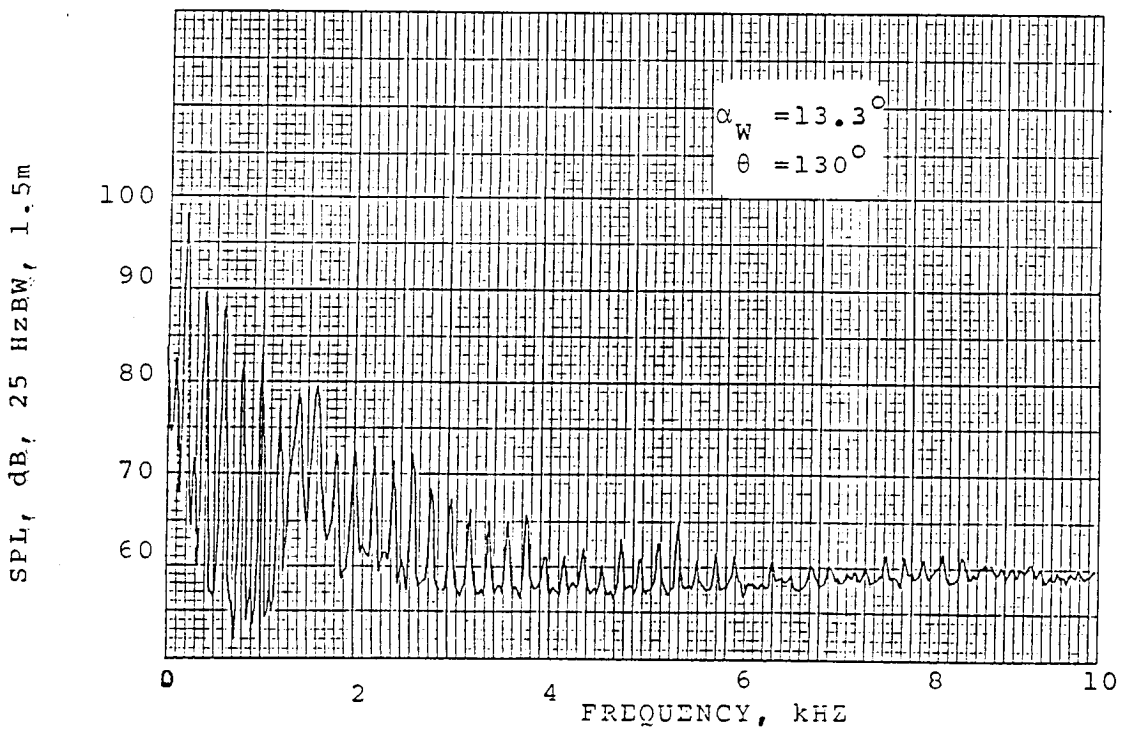

(2) PRESENT STUDY.

FIG. 3c: COMPARISON OF ACOUSTIC SPECTRA AT θ = 130°, α_w = 13.3°.

ORIGINAL PAGE IS
OF POOR QUALITY

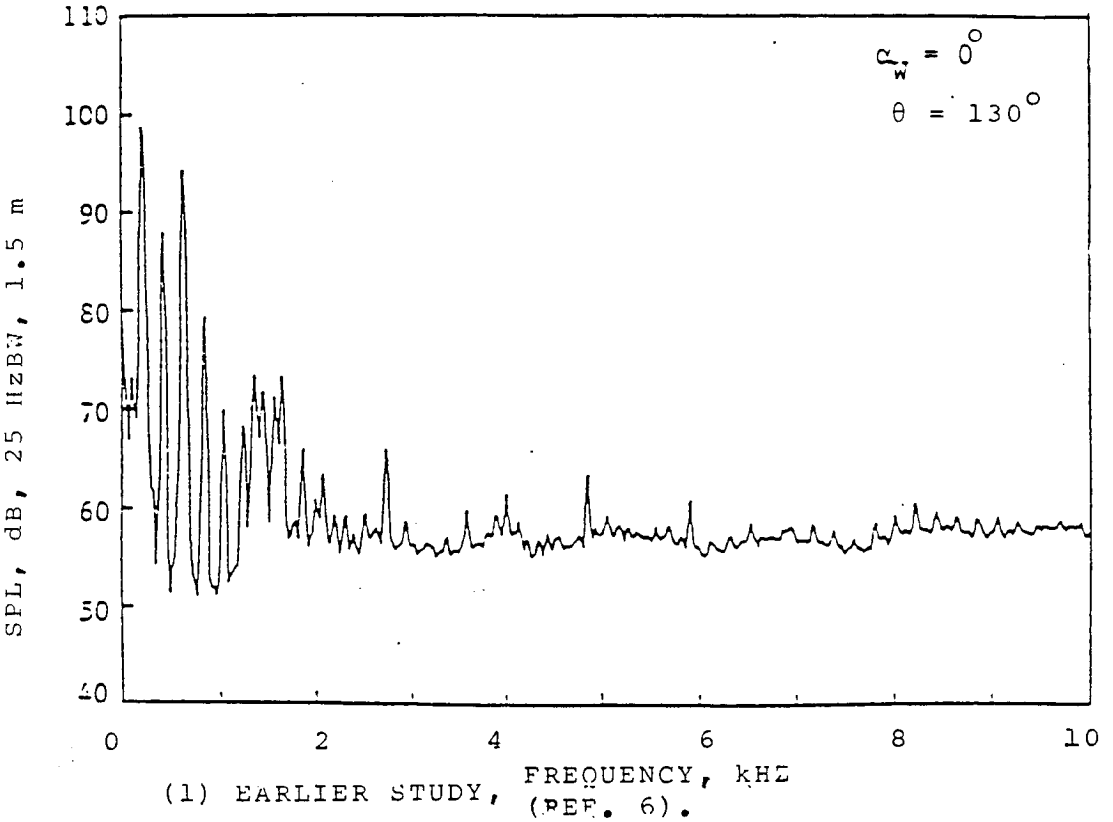

(1) EARLIER STUDY, (REF. 6).

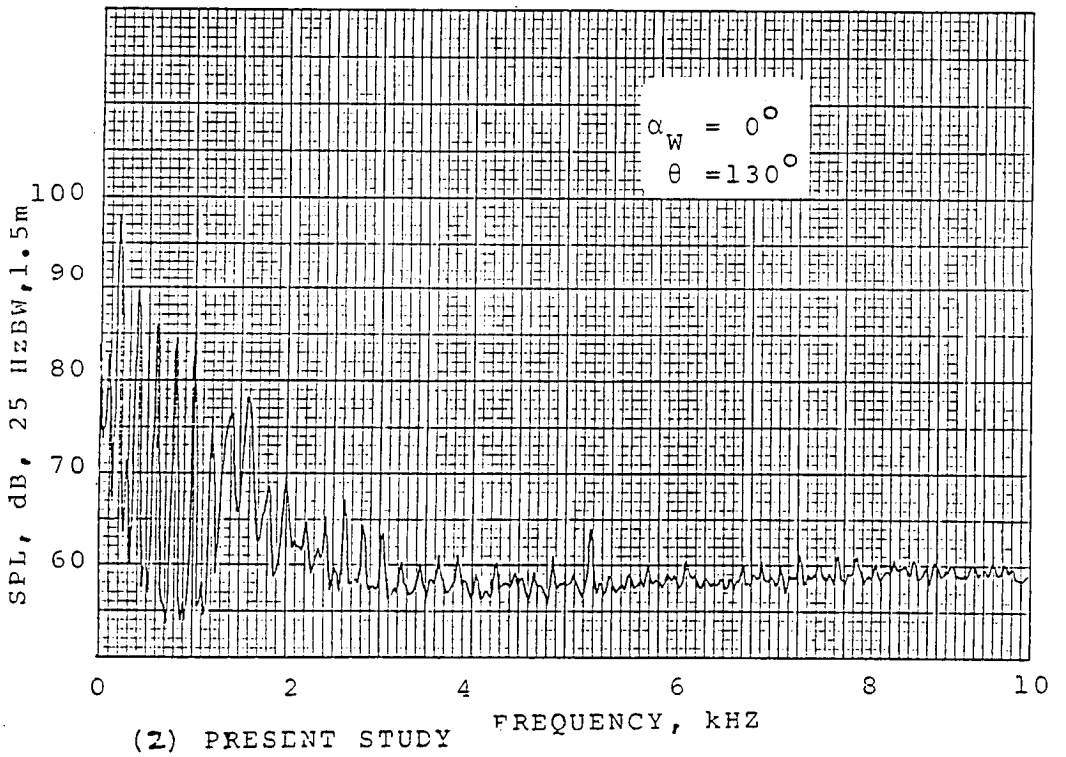

(2) PRESENT STUDY

FIG. 3d: COMPARISON OF ACOUSTIC SPECTRA AT $\theta = 130^\circ, \alpha_W = 0^\circ$

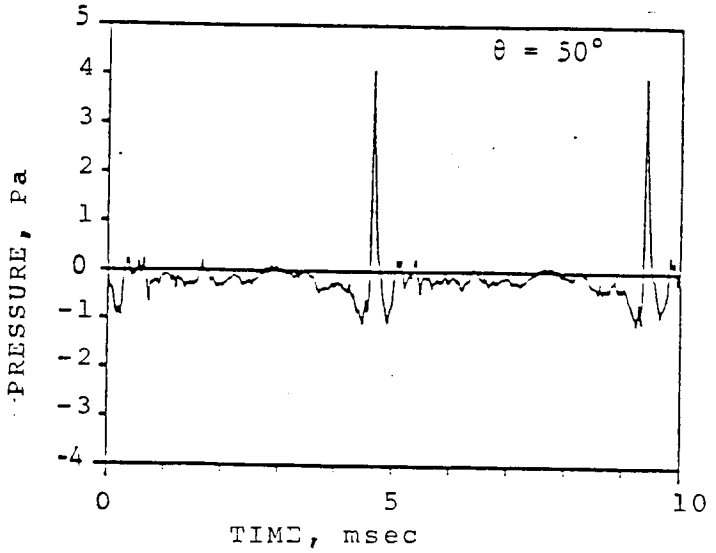

(1) EARLIER STUDY (REF. 6).

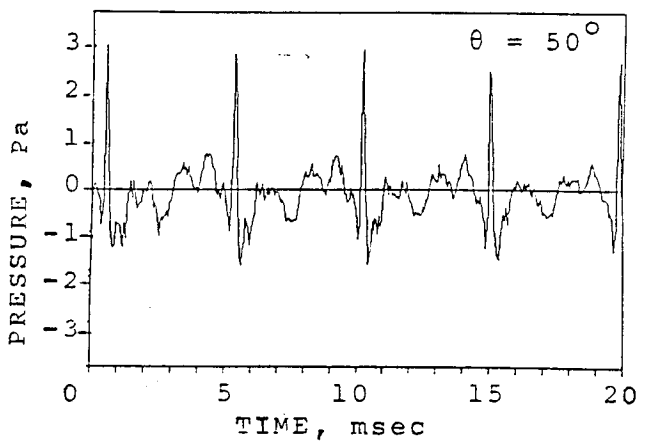

(2) PRESENT STUDY.

FIG. 3e: COMPARISON OF BVI SIGNATURES AT $\theta = 50^{\circ}$

ORIGINAL PAGE IS
OF POOR QUALITY

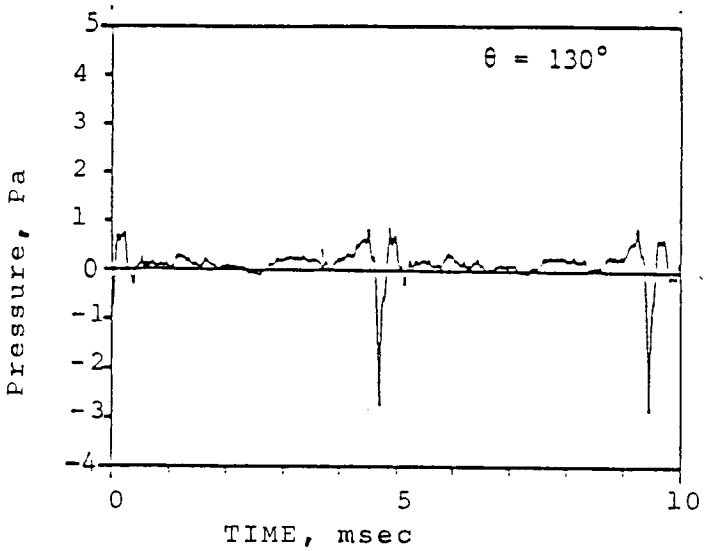

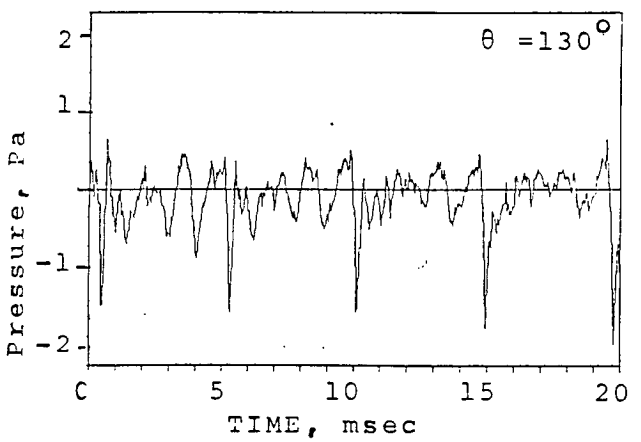

FIG. 3f: COMPARISON OF BVI SIGNATURES AT $\theta = 130^{\circ}$

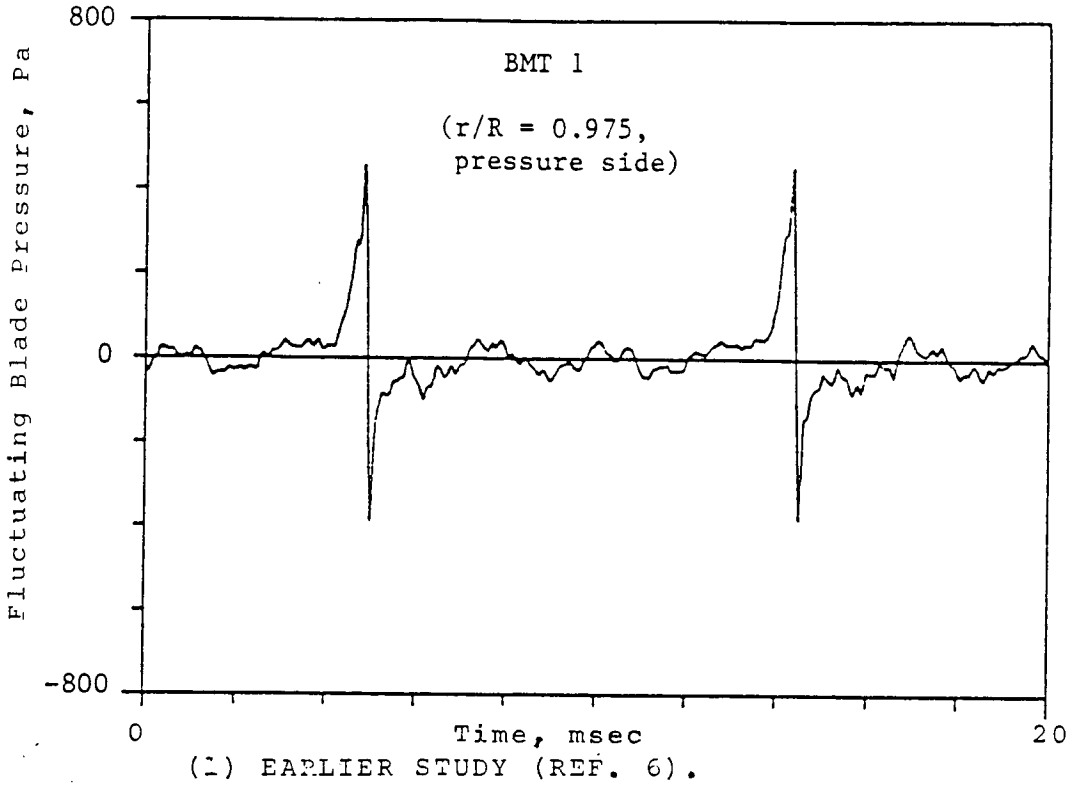

(1) EARLIER STUDY (REF. 6).

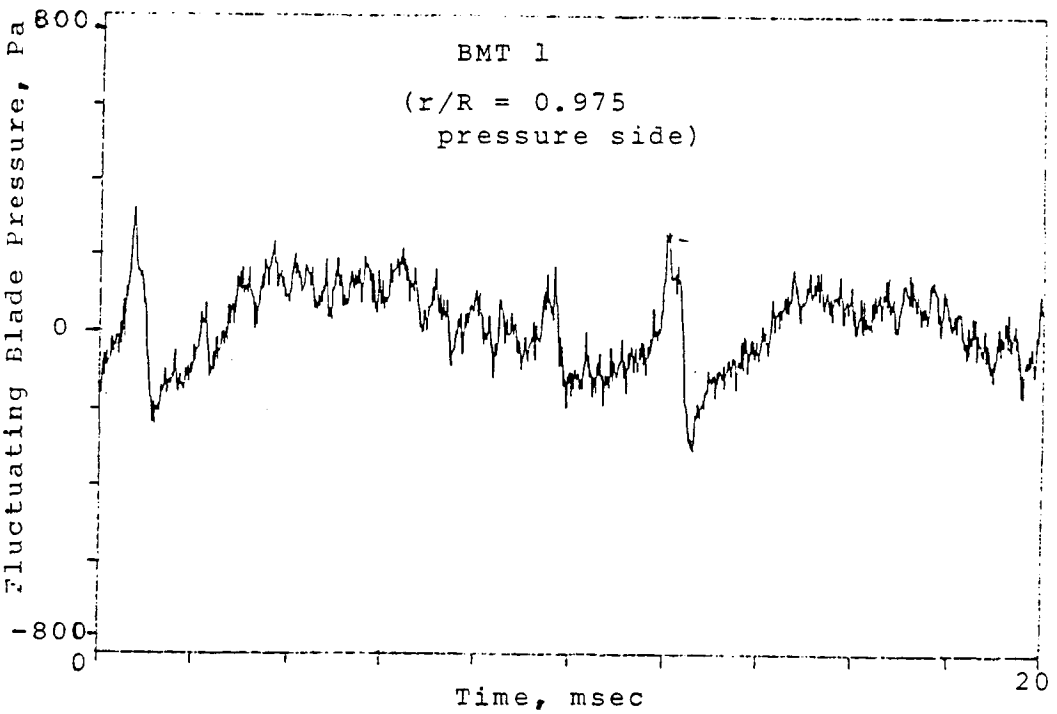

(2) PRESENT STUDY

FIG. 4a: COMPARISON OF BLADE SURFACE PRESSURES DURING BVI AT r/R = 0.975, PRESSURE SIDE.

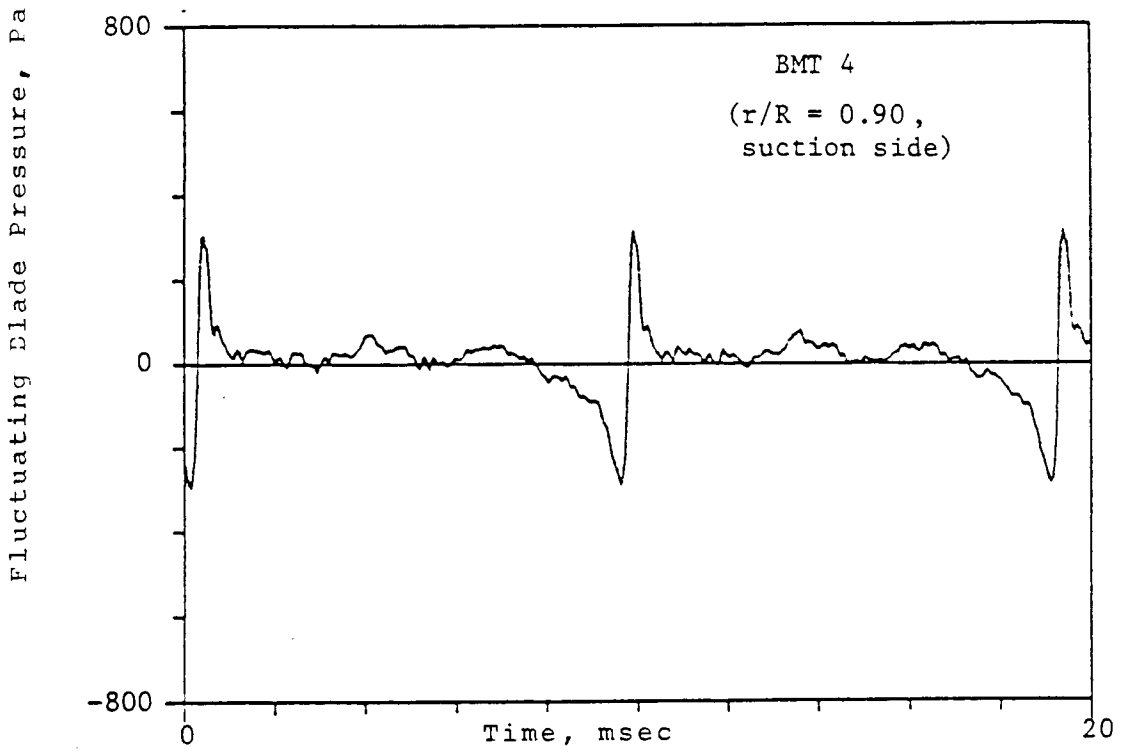

(1) EARLIER STUDY (REF. 6)

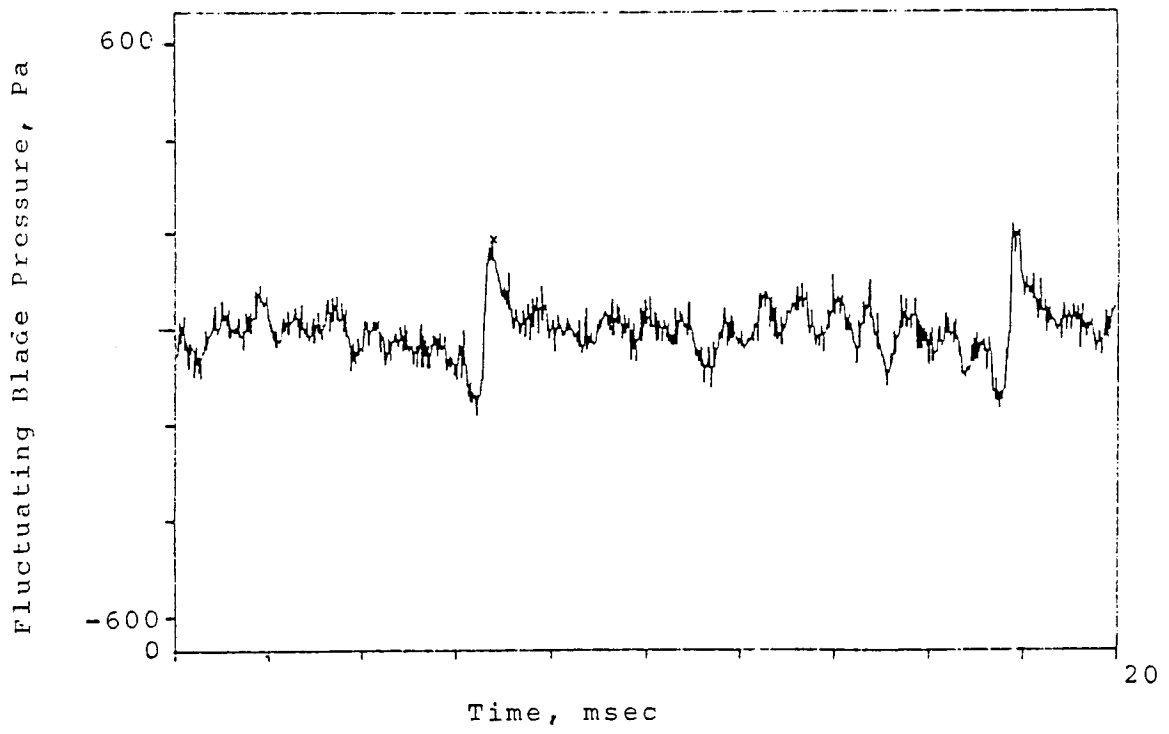

(2) PRESENT STUDY

FIG. 4b: COMPARISON OF BLADE SURFACE PRESSURES DURING BVI AT r/R = 0.90, SUCTION SIDE.

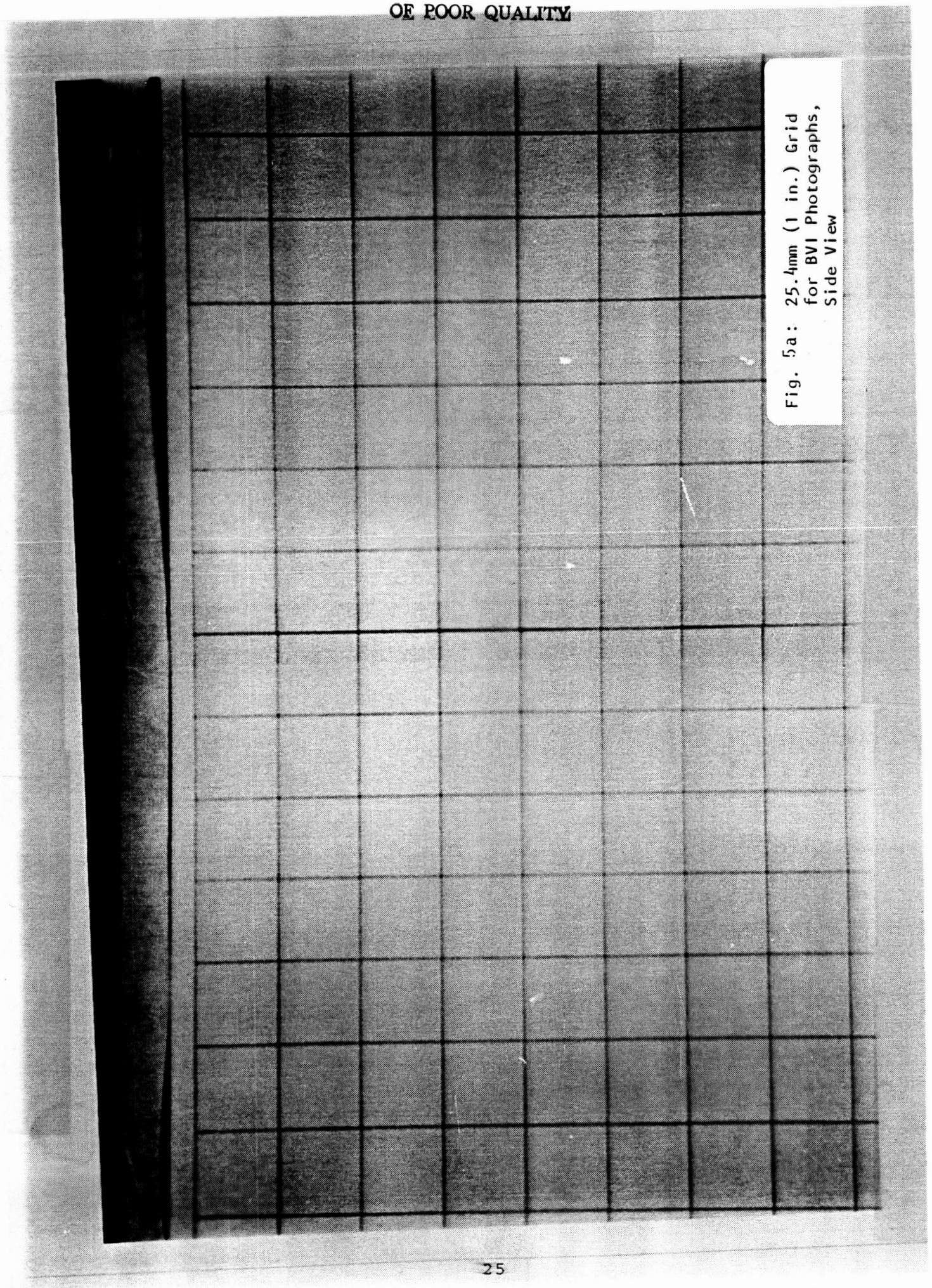

Fig. 5a: 25.4mm (1 in.) Grid for BVI Photographs, Side View

Fig. 5b: BVI at -5°, Side View

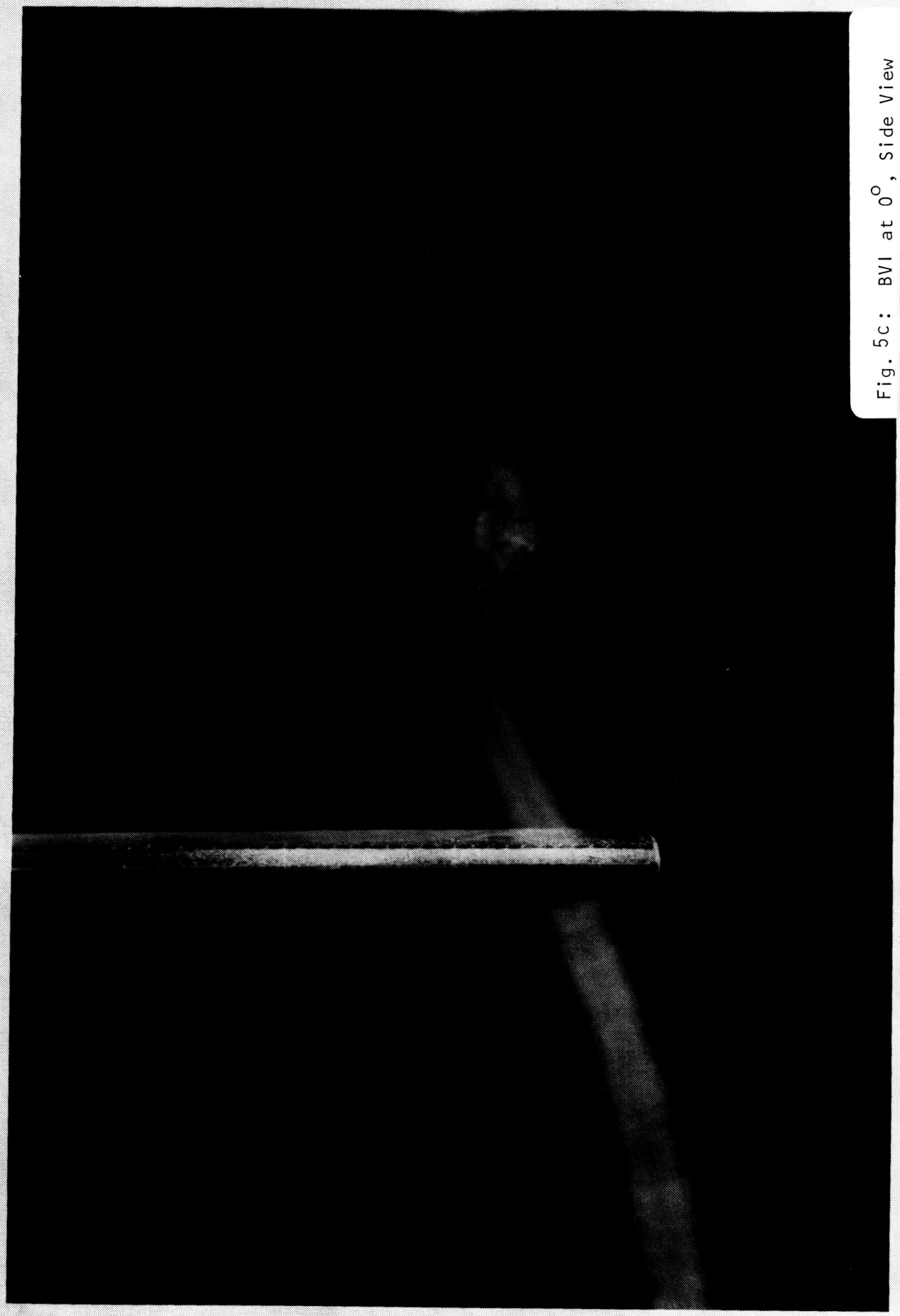

Fig. 5c: BVI at 0^{o}, Side View

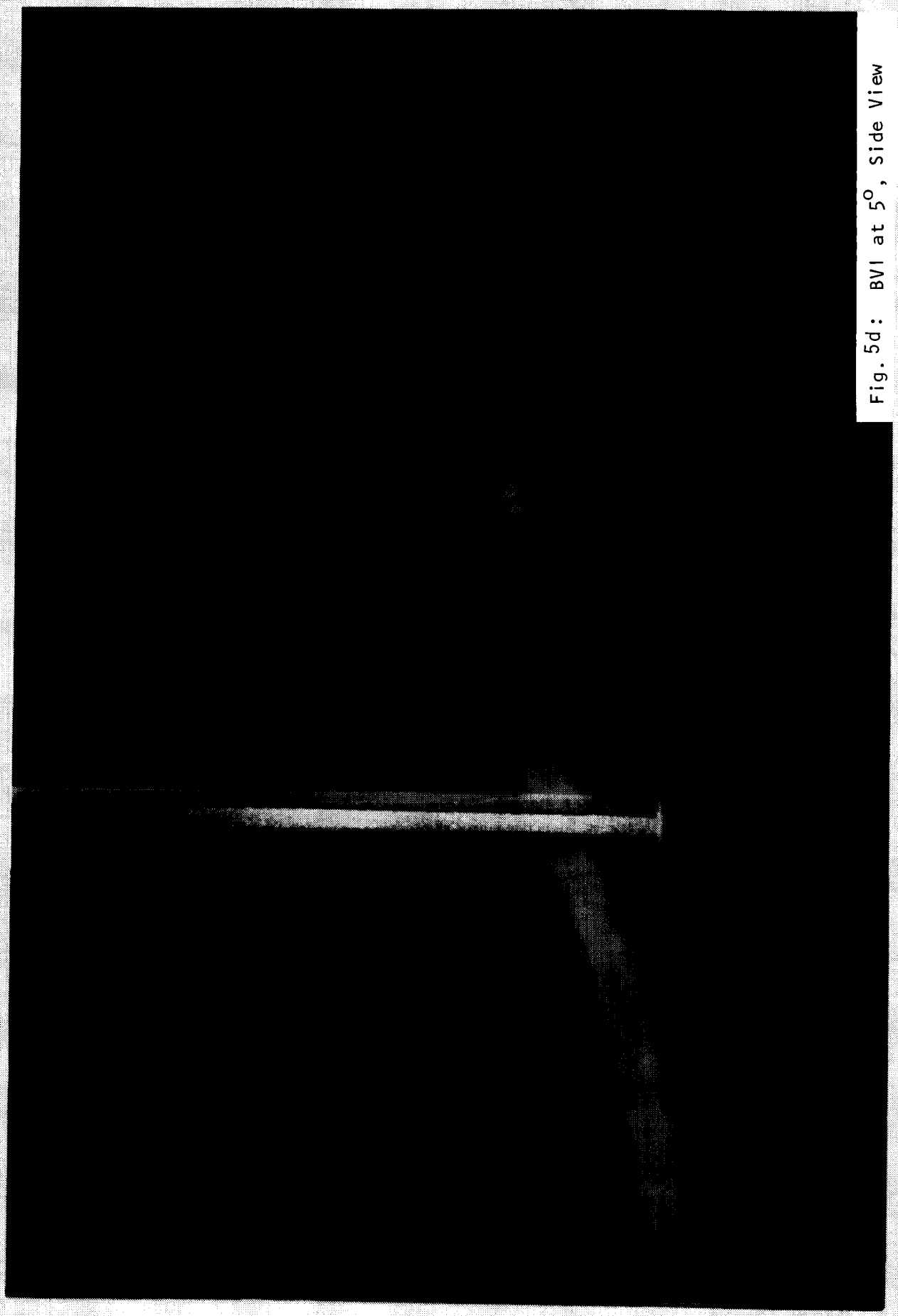

Fig. 5d: BVI at 5°, Side View

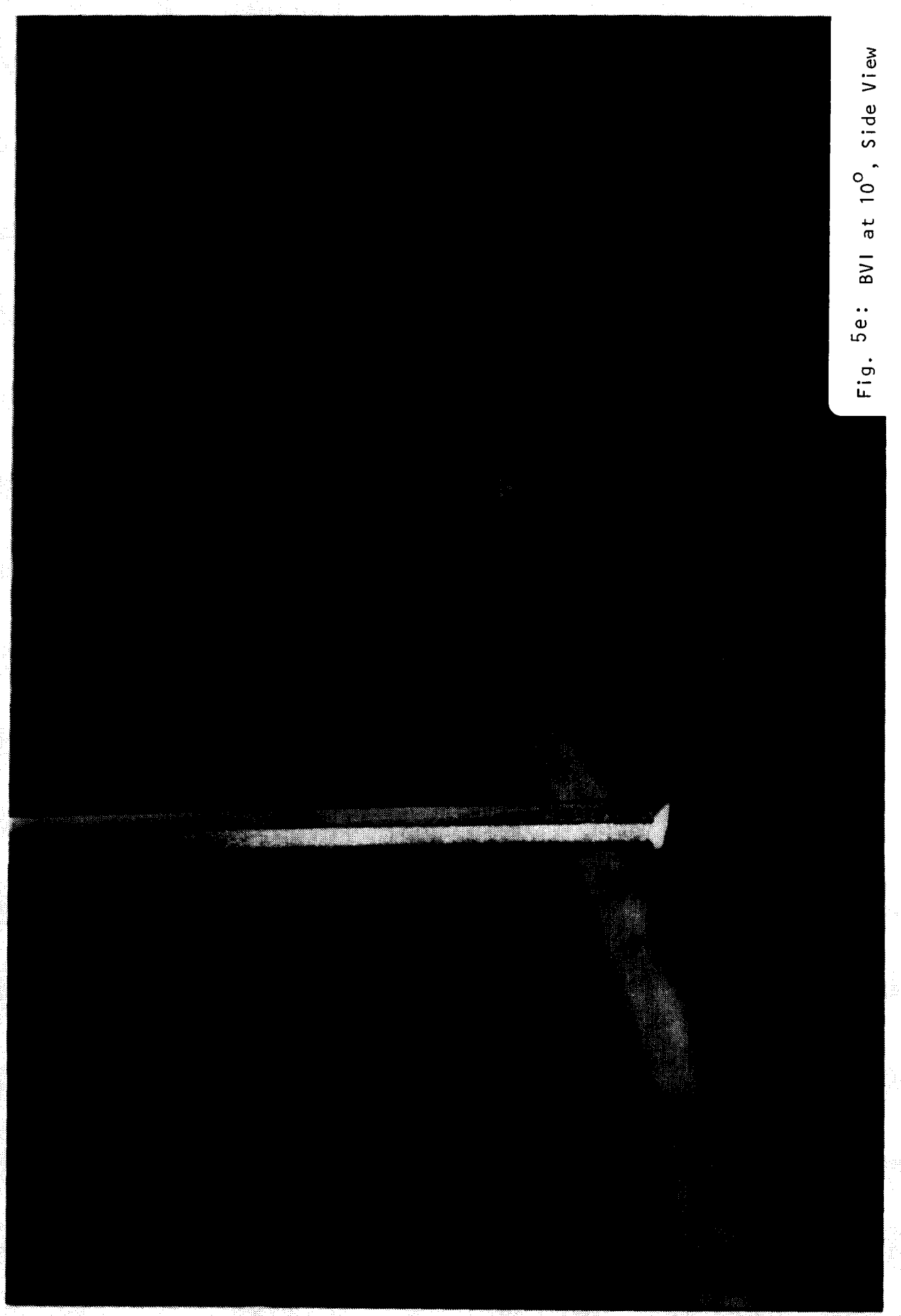

Fig. 5e: BVI at 10^{o}, Side View

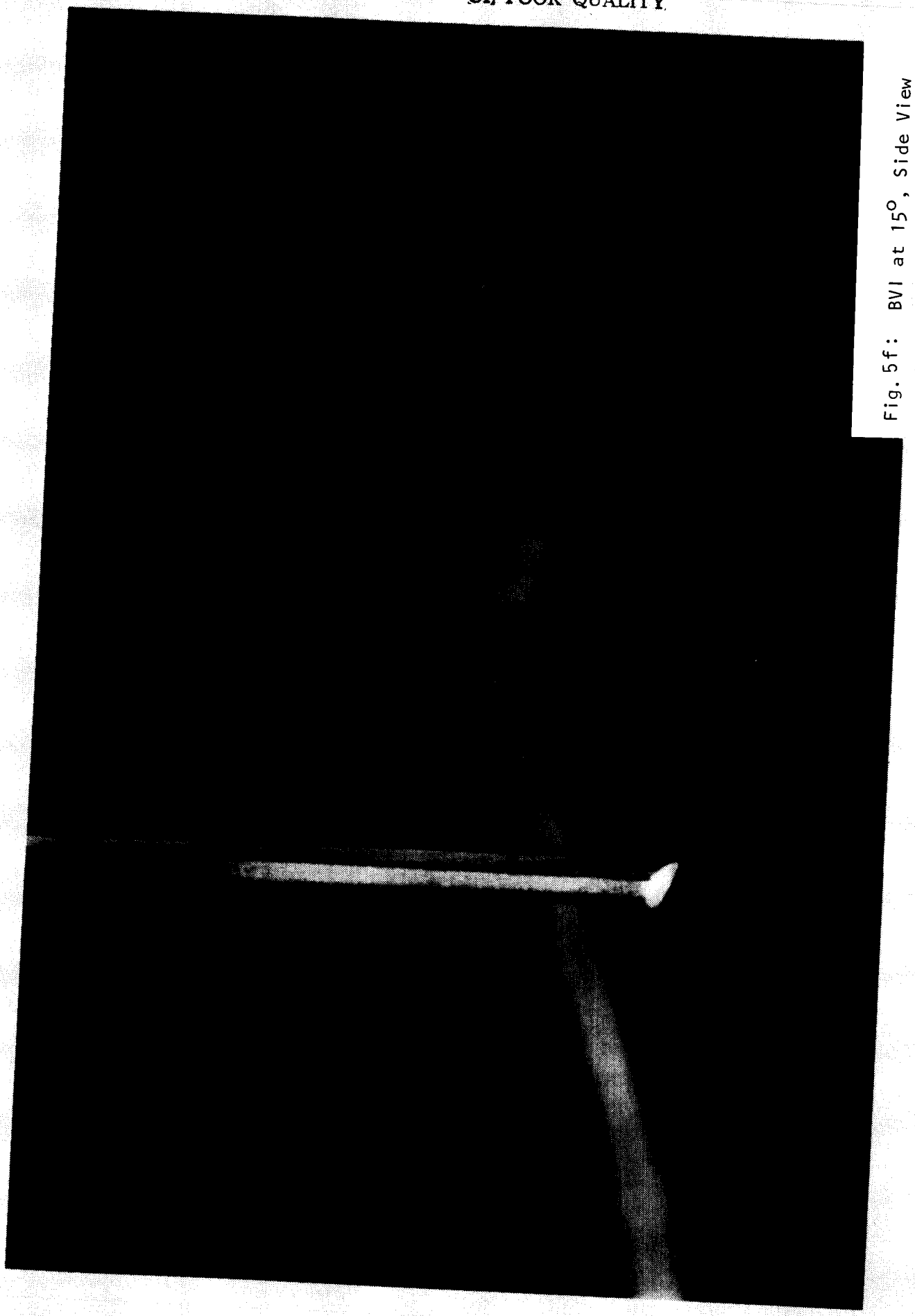

Fig. 5f: BVI at 15°, Side View

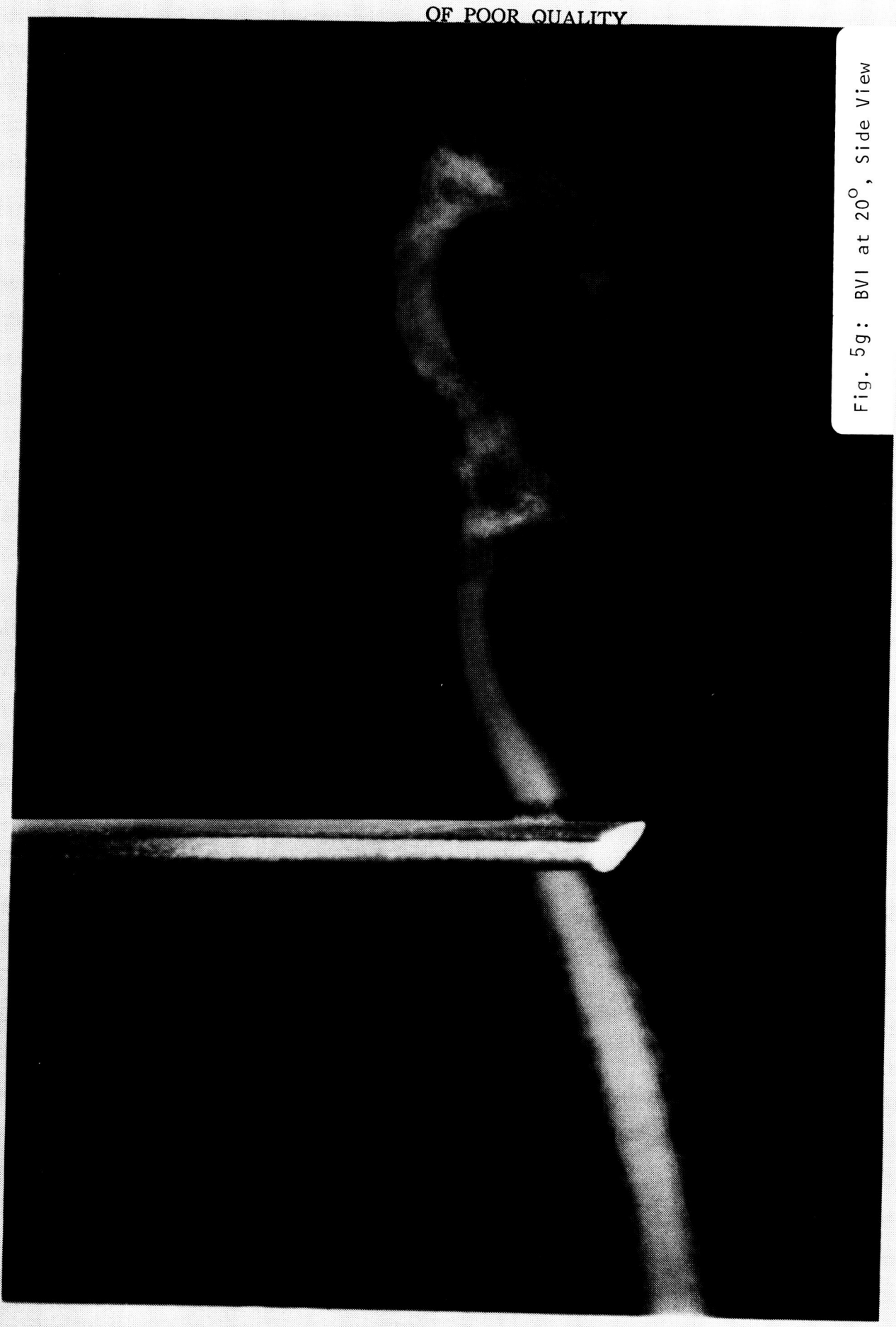

Fig. 5g: BVI at 20°, Side View

Fig. 5h: BVI at 30^{o}, Side View

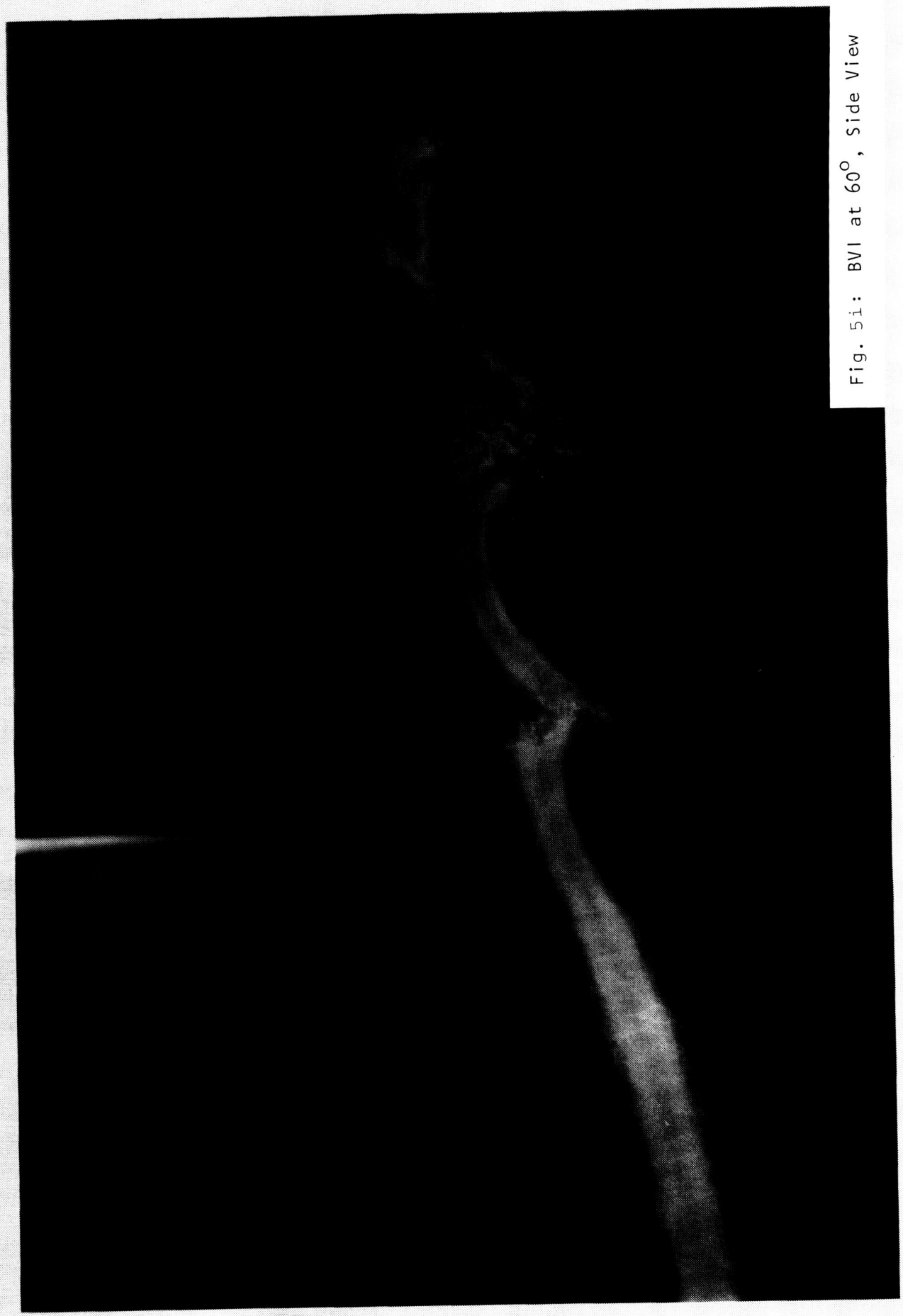

Fig. 5i: BVI at 60°, Side View

Fig. 5j: BVI at 90°, Side View

Fig. 5k: BVI at 120°, Side View